IEEE Access
Multidisciplinary | Rapid Review | Open Access Journal

Received October 24, 2018, accepted November 11, 2018, date of publication December 27, 2018,
date of current version January 16, 2019.

Digital Object Identifier 10.1109/ACCESS.2018.2889031

Directional Receivers for Diffusion-Based Molecular Communications

L. FELICETTI[1], M. FEMMINELLA[1,2], (Member, IEEE), AND G. REALI[1,2]
[1]Department of Engineering, University of Perugia, 06125 Perugia, Italy
[2]Consorzio Nazionale Interuniversitario per le Telecomunicazioni (CNIT), Italy

Corresponding author: M. Femminella (mauro.femminella@unipg.it)

ABSTRACT The particle motion in diffusion-based molecular communication systems is typically modeled by using Brownian processes. In particular, this model is used to characterize the propagation of signal molecules after their release from the transmitter. This motion cannot include directionality in the propagating signal and translates into omnidirectional broadcast communications. In order to make such molecular communications system suitable for supporting communications protocols at the molecular scales, we propose to improve the receiver capabilities by introducing a form of directionality while receiving biological signals. Inspired by the directionality introduced in electromagnetic communications by means of directional antennas, we designed a nanomachine receiver having directionality properties. Our aim is to increase the average concentration of signal molecules, also referred to as carriers, in the area around the receiver surface. In this way, it is possible to increase the signal strength at the receiver. For this purpose, we propose to use a purely reflecting shell to be placed at a configurable distance from the receiver surface. The shape of the shell can be modeled as either a spherical cap or a cylinder with an empty basis. The presence of this surface causes a number of signal molecules to remain trapped in a region close to the receiver surface for a sufficiently long time. In this way, the probability of assimilating additional carriers by the compliant receptors present on the receiver surface increases. By means of an extensive simulation campaign, we identified the most suitable configuration able to provide a significant advantage with respect to those not adopting the proposed solution. The resulting approach can be regarded as an enabler of protocols for diffusive molecular communications taking advantage of directionality properties at the receiver site. It can result in an increased communication range or in improved capabilities of discriminating signals of coexisting molecular communication systems.

INDEX TERMS Diffusion, directional receiver, molecular communications, receptors, reflecting shell.

I. INTRODUCTION

Molecular communication systems have recently attracted a lot of research efforts. They consist of (biological) nanomachines, staying within an aqueous environment, that exchange information over very short distances [27], [28]. To implement this type of communication, a transmitting nanomachine releases molecules in the surrounding environment. These molecules, also referred to as information carriers, act as communication signals. They propagate through the environment, where a receiver can capture them and decode the carried information. The signal reception typically happens as a chemical process which involves the signal molecules (ligands) and their compliant receptors distributed over the receiver surface. Bio-nanomachines can include biological components and are expected to implement elementary tasks. They need to be coordinated by means of signaling messages to be able to execute tasks of higher complexity.

Molecular communications can occur in different ways: those using diffusion-based channels are likely the most common and studied [27], since they are part of many natural phenomena. They are governed by pure diffusion propagation of information carriers [1], such as the one existing in the extracellular matrix of connective tissue. In some instances, diffusion is associated with the presence of a flow (advection-diffusion), which encompasses communications in the circulatory and lymphatic systems [2].

In this paper, we consider purely diffusive molecular communications. When carries are released from the transmitter, they can freely diffuse through the surrounding environment. This diffusion is similar to an isotropic propagation through

a radio channel. The motion of the information carriers in their path from the transmitting nanomachine to the receiving one can be modeled as a Brownian process, which does not include any directional component. Thus, it is more challenging to introduce directivity into the signal propagation process than in the case of advection-diffusion, since it is not possible to take advantage of any form of privileged direction of propagation of molecules. However, as witnessed by classic electromagnetic communications, directivity brings many advantages. In fact, for a given signal intensity, a directional receiver can support an increased communication range while providing reliability. Equivalently, for any given range value, a receiver with directional reception capabilities can have a better sensitivity, which can save a considerable amount of energy. Thus, if the necessary mean number of molecules to be received for reliably decoding a symbol is known, the use of a directional receiver can allow the transmitter to release less information carriers per symbol. This is a critical issue, since the amount nanoparticles available for signaling could be a limiting factor, due to restrictions on either the capabilities of nanomachines to store them, or their generation rate. Finally, the possibility to implement directional communications can help to implement spatial division multiplexing, thus allowing the coexistence of multiple molecular communications in the same area with minimal interference.

Thus, in order to take advantage of these features in the design of molecular communication protocols in diffusive environments, we focused on the receiver side. Our goal is to improve the communication range and the capability of successfully receiving biological signals in the presence of interference by providing the receiver with directivity capabilities. By inspiring to the conventional radio communications systems, we designed a mechanism to improve the received signal strength through a directional receiving antenna, able to increase the effective antenna surface and thus capture a larger number of information carriers, i.e. to increase the received signal strength.

The original research contribution of this paper consists in the design and performance evaluation of a receiving architecture with improved carrier capture capabilities. Our approach is to increase the concentration of the signal carriers in the area around the receiver, in order to facilitate further absorptions by compliant receptors. Since the receiver can be modeled as a sphere with a surface exposing a number of receptors, the number of received molecules can be increased by adding a reflector behind the receiver. This way, the reflecting shell will initially impede the signal molecules to escape by diffusion [1], and force a fraction of them to remain trapped close to the receiver surface for an additional time, before they escape anyway. This phenomenon increases the probability that some molecules would get in contact with free receptors present on the receiver surface and be assimilated. We have considered and analyzed two different shapes for the reflecting shell. The first one is a sphere cap, which exhibits a spherical symmetry all around the receiver (Figure 1.a-c). The other one is a cylinder with an empty basis (Figure 1.d). Clearly, the effectiveness of these solutions depends on the overall system size, such as the radius and the aperture of the cap, or the height of the cylinder. In general, a trade-off between entrapment and obstruction for any shell geometry exists. In fact, the more the shell covers the receiver, i.e., the smaller the aperture of the shell, the more it prevents carrier molecules from both entering into (obstruction effect) and exiting from (entrapment effect) the reception volume. In consideration of this trade-off, this paper analyzes the usage of different shapes of the shell.

We have analyzed the proposed receiving system through a simulation campaign, executed by means of the BiNS2 simulator [5], [6], [7]. From the analysis of results and the comparison with an ordinary receiver without the shell, for which also mathematical models exist [3], [4], we have identified the suitable system configuration in terms of aperture size of the shell and its distance from both the surface of the receiver, finding out a reasonable trade-off. With respect to our previous conference paper [22], we provided a more detailed system analysis. This includes a complete performance evaluation in terms of increased absorption and directionality as a function of system parameters, especially in the case of the cylinder shell, which results to be the solution with most interesting capabilities.

For molecular signals, the typical transmitter-receiver antenna duality property known for radio signals does not hold. Nevertheless, this work can also allow maximizing the expected benefits when used in conjunction with the directional transmitter proposed in [26], at least for short distances. Yilmaz *et al.* [26] proposed a similar approach (reflecting transmitter surface) for the transmitting side, following our preliminary work presented in [22].

The paper organization is as follows. Section II illustrates some background literature and related proposals on the subject. The system design is shown in section III, which highlights the rationale of the proposed architecture to improve the receiver capabilities. Section IV presents the numerical analysis of the proposed system, by focusing on received signal strength, delay spread of a single pulse of molecules, and sensitivity to misalignments. In addition, we optimize relative displacement of the receiver with respect to the shell, highlighting the underlying physical phenomena. Finally, in Section V we present our concluding remarks.

II. BACKGROUND AND RELATED WORK

Most of the literature in the field of molecular communications focuses on physical layer issues of different types of communication channels and media. Given the randomness of the diffusion-based channel, a critical issue is to set up reliable communications protocols at the physical and link layers before starting to develop those at the higher ones.

As for models relevant to pure diffusion [1], which is considered in this paper, an interesting review of transmission schemes can be found in [18]. The authors identify three general classes: pulse position modulation (PPM, [2]), concentration shift keying (CSK, [14]), and molecule shift

keying (MoSK), which consists of a combination of bursts of different molecules used for encoding signals. The receiver architecture proposed in this paper is quite general, and can be applied to all these different modulations.

As for the receiver model, we can distinguish between simplified models, such as those based on the so-called transparent receiver, and those a bit more realistic, where the receiver is able to absorb molecules. As for the first type, the transparent receiver is only able to count the molecules crossing its volume, without absorbing them and thus without removing them from the environment [11], [13], [15], [17]. As for the second type, most of proposals, such as [10], [12], and [19], assume that a sufficiently large number of receptors is exposed on the receiver surface, so that all molecules getting in contact the receiver are instantaneously absorbed (absorbing receiver model [3]). A slightly more refined model is presented in [4], where the surface of the receiver is assumed to be covered with a finite number of absorbing receptors. Thus, a molecule can be absorbed only upon hitting a compliant receptor. Hence, in these models, the stochastic nature of the ligand-receptor binding is not taken into account. In this regard, a step beyond is made in [8], which presents a model including also the trafficking time, roughly representing the molecule reception time. Finally, reversible binding between ligands and receptors is analyzed in [29]. In this work, we assume that a limited number of receptors cover the receiver surface in a homogeneous way, which is a typical assumption for such communication systems.

Other papers propose the solution of removing signal memory from the communication channel to reduce interference, by using enzymes [16], [25]. Although these approaches are different from ours, they can be combined together, since the mentioned enzymes can be used to flush the residual signal molecules within the shell volume.

Our initial idea of a spherical cap was re-used also in [23], where the authors use a system with joint signal and energy transfer. In addition, in [26] Yilmaz *et al.* analyze the performance of a transmitter with a reflecting surface, which in some way recalls our approach. The reflecting transmitter surface results to provide some directionality in the released signal, at least over short distances, with increasing directivity for larger transmitter size, due to a larger reflecting surface.

Finally, in [24] Guo *et al.* provide a nice analysis of the differences and the similarities between molecular and electromagnetic communications, considering also guiding structures.

III. SYSTEM DESIGN

A. SYSTEM MODEL

In our model, the receiver absorbs any carriers colliding with a free receptor (absorbing receptors, [4]), which is a quite common and realistic model (see also [29]). We consider a number N of absorbing receptors on the receiver surface, each one having circular shape with radius r_s. whereas the radius of the ligands is $r_c < r_s$. The receiver nanomachine is modeled as a sphere with radius r, whereas the transmitter one is modeled as a point source, as in [4]. The distance between the receiver center and the information carrier emission point is denoted as d. Carriers move according to the Brownian motion, with a diffusion coefficient in a three-dimensional space equal to $D = K_b T/(6\pi\eta r_c)$, where K_b is the Boltzmann constant, T the temperature of the aqueous medium, and η its viscosity.

The receiver model with absorbing receptors implies that any carrier colliding with one of them is immediately absorbed. Hence, the trafficking (absorbing) time is assumed to be negligible. This also implies that no busy receptors can be hit by carriers. Although this assumption introduces a degree of approximation, in the considered scenario it is acceptable, since the number of emitted carriers is much lower than the available receptors. Although very long simulations have been executed, it was never observed that a receptor absorbed more than a single carrier with the considered system parameters. This confirms that our assumption is acceptable in the considered scenario.

The above system can be modeled by the following equations in spherical coordinates (ρ, ϕ, θ), with origin of coordinates co-located with the center of the receiver. As for the emission of nanoparticle, the point transmitter emits the information molecules at $t = 0$. The Fick's diffusion equation describes the propagation of the information molecules in the environment:

$$C(\rho, t \to 0|d) = \frac{1}{4\pi d^2}\delta(\rho - d), \tag{1}$$

where $C(\rho, t \to 0|d)$ is the molecule distribution function at time $t \to 0$ and distance ρ with initial value d. The first boundary condition is

$$\lim_{\rho\to\infty} C(\rho, t \to 0|d) = 0, \tag{2}$$

that is, for any time, the molecule distribution function will vanish for very large distances from the emission point. The Fick's second law describes their propagation in a 3D environment [1], [4]:

$$\frac{\partial C(\rho, t|d)}{\partial t} = D\nabla^2 C(\rho, \phi, \theta, t|d) \tag{3}$$

As mentioned above, the receiver can absorb the signal molecules by means of surface receptors. This phenomenon can be modeled by means of an absorption rate k_1, which depends on the chemical affinity between signal molecules (ligands) and receptors, as well as their number and size, according to the relationship:

$$k_1 = \frac{N r_s D}{\pi r^2} \tag{4}$$

The absorption reactions that occur on the receiver surface give the second boundary condition on the molecule concentration:

$$D\frac{\partial C(\rho, t|d)}{\partial \rho}\bigg|_{\rho=r^+} = k_1 C(r, t|d) \tag{5}$$

The change in absorbed concentration over time is equal to the flux of the diffusion molecules through these surface receptors. This process can be modeled by the following equation:

$$\frac{\partial C_a(t|d)}{\partial t} = D\frac{\partial C(\rho, t|d)}{\partial \rho}\bigg|_{\rho=r^+}, \tag{6}$$

where $C_a(t|d)$ is the average concentration of absorbed molecules by the surface receptors at time t. Combining (5) and (6), we can obtain the radiation boundary condition, which shows that the equivalent absorption rate is proportional to the surface molecule concentration:

$$\frac{\partial C_a(t|d)}{\partial t} = k_1 C\left(r, t|d\right). \tag{7}$$

At time $t = 0$, there are no information molecules at the receiver surface, so the additional initial conditions are

$$\begin{cases} C\left(r, 0|d\right) = 0 \\ C_a\left(0|d\right) = 0. \end{cases} \tag{8}$$

The number of absorbed molecules at time t upon the release of a burst of Q molecules is equal to

$$A\left(t\right) = A\left(t|d\right) = 4\pi r^2 QD \int_0^t \frac{\partial C(\rho, \tau|d)}{\partial \rho}\bigg|_{\rho=r^+} d\tau. \tag{9}$$

B. DIRECTIONAL RECEIVER ARCHITECTURE

Under the mentioned assumptions about the receiver, the proposed overall directional receiving system includes a signal reflector positioned behind the receiver, i.e. in the opposite position with respect to the transmitter. As mentioned above, in this paper we consider two shapes for the reflecting shell: a spherical cap (Figure 1.a,b,c) and a cylinder (Figure 1.d).

The first one is a sphere cap of radius R, which exhibits a spherical symmetry all around the receiver, having all the walls of the shell at constant distance from the receiver $R-r$. The other is a cylinder with an empty basis (Figure 1.d), with height H and radius of the basis R. The distance between the walls of the shell from the receiver, located in the center of the cylinder, is not constant, since it can be either closer to the basis opposite to the entrance ($s_1 = H/2 - r$) or to the lateral wall ($s_2 = R - r$), with a maximum distance $s_3 = \sqrt{(H/2)^2 + R^2}$. For any other position of the receiver, the above equations have to be adapted by the resulting offset from the center of the cylinder.

Before entering into the details of the characteristics of the two different receiving systems, let us focus on the rationale of our proposal. The usage of a reflecting shell increases the effective surface of the receiver ''antenna'', (corresponding the actual receiving surface hit by carriers), by avoiding a significant fraction of the signal to pass over and conveying it towards the receiver surface, similarly to what is done by a dish antenna in radio communications. Differently from the electromagnetic counterpart, a molecule hitting the reflector does not follow a deterministic path back to the receiver surface. Nevertheless, the presence of the reflector represents

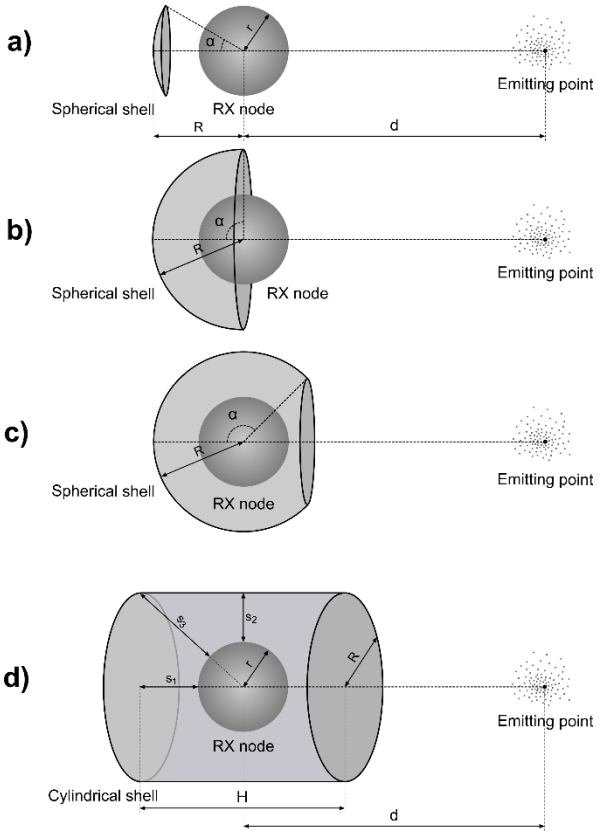

FIGURE 1. Reflecting shell layout for a directional receiver.

an obstacle for molecules, which need to come back to the shell aperture to move away following the Fick's law. Thus, the goal of the reflecting shell is to prevent carriers from quickly moving away from the receiver, due to their motion described by the law of diffusion. Although this effect cannot be totally avoided, the net effect of the presence of the shell is to trap carriers for a sufficiently long time around the receiver, so as to significantly increase the collision probability with receptors.

The idea of placing a reflecting shell downstream the receiver comes from the observation of the reception pattern observed by using a receiver without any shell, as the one shown in Figure 2.a.

This figure shows the so-called absorption map, which is a scatter plot, on the surface of the receiver, indicating the coordinates of all its receptors. The small points show the positions of receptors that have not absorbed any molecule, whereas the thicker points indicate the receptors that have absorbed a molecule. The abscissa axis reports the longitude ϕ of receptors' position (in radians, in the range $]-\pi, \pi]$), and the ordinate axis reports their latitude θ (in radians, in the range $[-\pi/2, \pi/2]$). The coordinate (0,0) indicates the direction connecting the emission point with the center of the receiver, and represents the center of the front side of the receiver. It is evident the most of nanoparticle absorptions happen in the front side of the receiver. This is the region nearest to the emission point, thus the most favorable one for

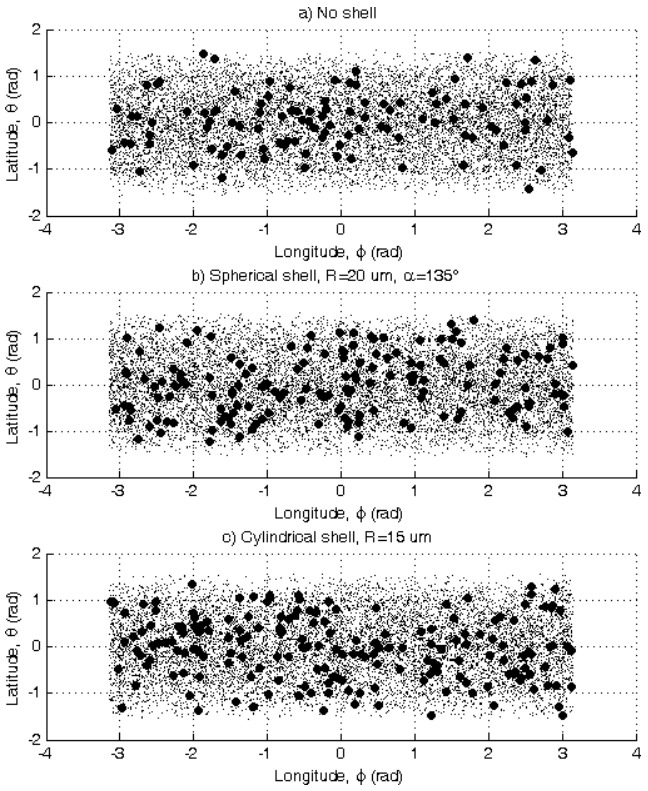

FIGURE 2. Absorption map at time 10 s for a) standard receiver without any reflecting shell, b) spherical shell (R = 20μm and $\alpha = 135°$), and c) cylindrical shell (R = 15μm and H = 30μm).

absorptions, which are more likely to happen for receptors at small distances (see also [4, eq. (6)]). Indeed, upon the transmission, the diffusion pushes nanoparticles to escape from the emission point and thus also towards the receiver. Although some nanoparticles are absorbed also by receptors in the opposite side of the receiver (i.e. those with longitude close to π or $-\pi$) due to their Brownian movement, the law of diffusion tends to push them away from the emission point, thus not favoring further absorptions.

Thus, our idea is to make use a shell to trap some of the information carriers that have passed beyond the receiver position, but are still close to it. Putting a reflective barrier on their path leading them far from the emission point, and given their random movement, we increase the probability that some particles hit the shell when moving back towards the receiver to find an escape.

The whole system is symmetric with respect to the axis connecting the transmitter to the center of the receiver. As mentioned above, in this paper we consider two shapes for the reflecting shell.

The first shape is a spherical cap, with radius $R > r$ and aperture angle α, as illustrated in Figure 1.a-c.

When α equals 90° (Figure 1.b), the shell embraces half receiver, whereas for larger aperture angles the entire receiver may be contained within the shell (Figure 1.c, with $\alpha = 135°$). In this case, the system shape offers an aperture that allows carriers entering the area surrounded by the shell. The center of the spherical cap is co-located with the receiver center.

Given the shape of the shell, all the points of its wall are at a fixed distance from the receiver surface. For this reason, it is expected that its shape favors a homogeneous absorption of molecules by all surface receptors.

From a mathematical viewpoint, the presence of the spherical shell can be modeled by adding the following boundary conditions to the equations (1) – (8):

$$\begin{cases} D\dfrac{\partial C(\rho,t|d)}{\partial \rho}\Big|_{(R^-,\phi,\theta)\in\Omega^-} = 0 \\ D\dfrac{\partial C(\rho,t|d)}{\partial \rho}\Big|_{(R^+,\phi,\theta)\in\Omega^+} = 0 \end{cases}, \tag{10}$$

where the reflective nature of the shell can be modeled with a zero absorption through its surface Ω, considering both particles hitting it from inside (Ω^-) and outside (Ω^+), whose coordinates are characterized by a fixed distance R from the receiver center. Now, also coordinates ϕ and θ need to be accounted in equations, since part of the original symmetry of the system is lost.

The second shape is a cylinder. In this case, the axis of this cylinder corresponds to the direction connecting the receiver center with the transmission site. The basis of the cylinder facing the emission point is open in order to let the carriers enter the structure. In contrast, the other basis is closed, in order to inhibit the carriers staying within the cylinder volume to exit from it and to force them to randomly move inside this volume. This increases the probability of collision between the entered carriers with the surface receptors of the receiver. Let H and R denote the length and the radius of the basis of the cylinder, respectively. We assume that the cylindrical shell completely contains the receiver in it, their centers being co-located. We have initially set $H = 2R$ and then relaxed this constraint in order to carry out a more general analysis, allowing the receiver to be closer to the aperture or to the basis opposite to the entrance side. As for the boundary conditions describing the reflecting nature of the cylindrical shell, they can be derived in similar way to those presented for the spherical cap in (10).

For both considered shells, the spherical cap and the cylinder, the distance d between the center of the receiver and the carrier transmission site is the same.

C. IMPLEMENTATION ISSUES

Some practical implementation issues to realize the proposed system exist. First, it is necessary to design a mechanism to connect the shell with the receiver. In Figure 1, the connection between the receiver and the shell is omitted for the sake of neatness. This connection could be implemented in different ways. The simplest one is to use adhesive molecules deployed on a protrusion, which connects them. If the connection is solid enough, the receiver could even rotate towards the transmitter direction in order to maximize the projection of the shell aperture over the plane orthogonal to the line connecting it with the transmitter. This rotation would produce the

largest gain (maximum number of received molecules in the observation time) thus implementing a true directive system.

Finally, it is worth noting that structures similar to the shells considered here, with a size of a few μm, already exist in nature. An example is the glass shell of some micro-algae reported in [21]. Thus, the overall system seems easily feasible by using already available structures.

IV. PERFORMANCE EVALUATION

This section presents the performance analysis of the proposal. We focus on two aspects. The first one is the performance improvement over the reference system, which is a receiver without any reflector. The second one is the signal delay spread evaluated at the receiver site, since it strongly affects inter-symbol interference (ISI), which has a considerable impact on the achievable symbol rate. Finally, we also analyze the performance sensitiveness to misalignments of the shell due to rotation errors, in order to assess its directional capabilities.

TABLE 1. System and simulation parameters.

Symbol	Description	Value
Δt	Simulation time step	0.1 µs
t	Simulation time	seconds
T	Temperature	310 K
e	Coefficient of restitution	0.95 [9]
η	Viscosity of the aqueous medium	0.0011 Pl [9]
r	Radius node	2.5 µm
R	Shell radius (sphere/cylinder)	5, 10, 15, 20 µm
α	Aperture of the spherical cap	30°, 60°, 90°, 135°
H	Length of cylinder	2 R
N	Number of surface receptors	10000
r_s	Radius of surface receptors	4 nm
r_c	Radius of emitted molecules	1.75 nm
d	Distance between TX and RX centers	26.5 µm
Q	Carriers burst size	2000
L	Side of the simulated space	1 mm
L_F	Length of the front branch of the cylinder	0, 2.5, 7.5, 12.5, 17.5, 22.5 µm
L_B	Length of the bottom branch of the cylinder	0, 2.5, 7.5, 12.5, 17.5, 22.5 µm
β	Rotation angle for the cylindrical shell	45°, 90°, 180°

The analysis has been done by using the BiNS2 simulator, which is a well assessed simulator of molecular communications systems [5]–[7]. Table 1 lists the simulation parameters used in the experiments. The simulation environment is modeled as a wide cubic space, with side L. The transmitter and the receiver are located near to the center of the simulation environment. If a nanoparticle hits the inner surface of the cube, it is removed from the simulation. We used a value of L large enough to consider possible removal of carriers having negligible effects on simulation results. In fact, for very large values of L, the probability that a nanoparticle at the border of the simulation environment could come back by diffusion and hit the receiver is actually negligible.

The advantage of using a cubic space instead of an infinite one is that it allows partitioning the simulation environment in a finite number of cubes. This is done by applying the *octree* simulation data management introduced in [7], which allows scaling the simulation time down.

The minimum value of the side of each sub-cube is equal to 62.5 μm. In addition, we have enforced that the receiver with its shell is always contained within one of the octree sub-cubes, in order to avoid border effects.

We used the partially inelastic model to manage the collisions of nanoparticles with the shell. When a collision occurs, we compute the effects of a partially elastic collision with the plane that is tangent to the shell in the collision point. This is independent of the shape of the shell and on the initial position of the nanoparticle (within the volume embraced by the shell or in the external environment).

In this paper we do not report the equations used to manage collisions, since their detailed description can be found in our previous paper [6]. In that manuscript, we introduced the cylindrical domain for modeling the endothelium of blood vessels, thus the extension to model the collisions with a shell is straightforward. We have not modeled the shell thickness, since due to the Brownian motion of the nanoparticles it has a negligible impact on the simulation results, which mainly depend on the number of carriers colliding with the shell surface facing the receiver. Finally, our simulations account also for collisions between nanoparticles, since in small volumes close to the receiver site their effect could have an impact on simulation results.

In our experiments, when the transmitter emits carriers, it instantaneously releases a burst of $Q = 2000$ carriers.

A. EFFECTIVENESS OF DIFFERENT SHAPES

Figure 3 shows the total average number of absorber carriers for different configurations, at the simulated time $t = 10$ s. The abscissa values are the shell radius R, whereas the bar color identify the aperture angle α. The red dashed line shows the theoretical value for the reference system (receiver without shell), evaluated as in [4]. As for the proposed system with a reflector, first let us focus on the spherical one. The aperture angle of 30° seems to not have any positive effects, independently of the value of the shell radius. For increasing values of α, such as 60°, the behavior is similar. The main comment is that in both configurations the reflecting shell lies completely behind the receiver (see also Figure 1.a). The resulting effect is that the reflector has a negative effect, since it hampers carriers that have reached positions beyond both the receiver and the shell to come back and collide with the back surface of the receiver relative to the position of the transmitter. In fact, although less frequent, some absorptions in the reference system can occur also in this region (see Figure 2.a). However, it does not implement an effective trap to keep some carriers close to the receiver surface and thus increases the number of absorptions in that region of the receiver surface, which is the target of our proposal.

For an aperture of 90°, the performance begins to be sensitive to the radius of the shell R, although it does not still provide any performance improvements. For small values

of R, the effect on the absorption process appear, and it improves with it. In fact, for increased values of R, the space between the receiver and the shell, where the particles can enter the shell volume, becomes larger. These nanoparticles remain trapped for a while behind the receiver, and have a higher chance of being absorbed. This phenomenon balances the fact that the particles behind the shell cannot easily reach the receiver.

Finally, for the aperture equal to 135°, the dependency on R is clear. The system is significantly hampered by small R values, but performance improves when the value of R increases, and the performance gain with respect to the reference system becomes significant for $R = 15$ μm (about further 20% absorptions) and further improves (about 60%) for $R = 20\mu$m. The rationale underlying this behavior is clear: due to the small value of the shell radius, also the aperture of the system is very small (see Figure 1.a), thus causing a small number of carriers entering the shell volume. When R increases, not only the aperture is larger, but it gets also closer to the emission point, where the concentration of nanoparticles is higher. Thus, a large number of carriers tend to enter the shell volume by diffusion. Once carriers are inside this volume, the shell wall traps them for a significant amount of time, depending on shell size and shape, thus increasing the chances for hitting the surface receptors of the receiver and thus increasing the number of absorptions. This is particularly evident for the receptors located in the portion of the receiver surface opposite to the emission site.

This improvement is very important for large R values, because it completely balances the apparent limitation that the particles can enter in contact with the receiver just by entering the shell volume through the front side. Moreover, for $R = 20$ μm, it definitely outperforms the reference system. However, since the aperture is large and not very close to the receive surface, after a while some of them can exit the shell volume without being absorbed.

This means that, in the end, the presence of the shell does not increase the average amount of molecules present in the surrounding space (channel memory) in the long run, which is known to cause ISI, since it could interfere with possible future transmissions. This concept is further detailed and supported by numerical results and comments to Figure 5.

Let us now consider the cylinder. We have used three values for R(5, 10, and 15 μm), with the largest one producing an aperture of approximately the same size and distance from the emission site that characterize the spherical cap with $R = 20$ μm and $\alpha = 135°$. In this way, we can have a fair comparison with that configuration, which is the one providing the best performance in terms of absorbed nanoparticle for the spherical cap.

Similarly to the spherical cap with $\alpha = 135°$, the cylindrical shell with the smallest radius does not provide satisfactory results. In contrast, the improvements for $R = 10$ μm and 15 μm are significant, with almost a 3 dB gain for the largest radius. Given the system size, we expect that the number of carriers entering the trapping structure is similar

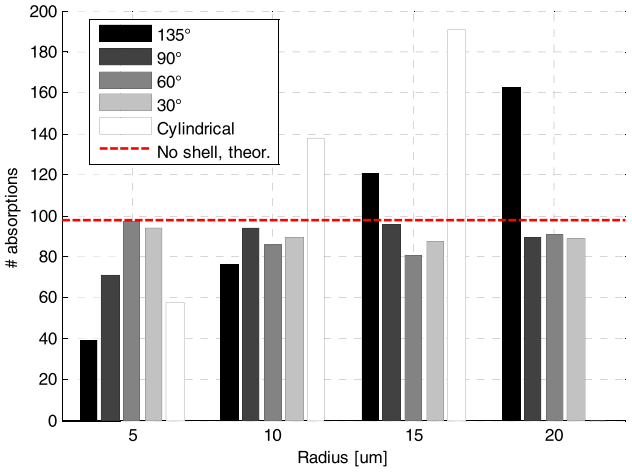

FIGURE 3. Average number of absorptions as a function of shell radius, for different configurations. The simulation time is equal to 10 s.

to the case with the spherical cap shell with the largest size ($R = 20$ μm and $\alpha = 135°$). However, being the minimum distance between the cylinder surface and the receiver lower than in the spherical cap case, these carriers happen to be absorbed more frequently, since their chances to hit the receiver increase.

In the case with $R = 15$ μm, even if the distance between the cylinder walls and the receiver is higher, the number of carriers that enter the shell volume is also higher and, for those going beyond the receiver, the only way to exit the system is returning back towards the aperture. This provides further chances for them to be absorbed by the surface receptors, due to their Brownian motion.

We have also executed some tests by using larger values of the distance between the emission point and the receiver center. For these tests, we have used the maximum values of the radius for both the spherical ($R = 20$ μm) and the cylindrical shells ($R = 15$ μm), since they are those providing the best performance. The results show that the gain due to the use of the shell remains substantially constant as d increases. For the cylindrical case, it is nearly 3dB, even for the highest simulated distance $d = 57$ μm, which represents approximately twice the minimum default distance of 26.5 μm, as shown in Figure 4.

We now focus on the best two configurations identified above, that is the spherical cap with $R = 20$ μm and $\alpha = 135°$, and the cylinder with $R = 15$ μm. If we observe the absorption patterns in Figure 2.b-c, we can see that the improvement is essentially due to a larger number of absorptions happening in the back part of the receiver, which is close to a longitude of 180°, due to the trapped molecules behind the receiver. This proves that our initial intuition is correct.

Furthermore, if we examine the temporal absorption patterns for the reference system and for those two configurations (Figure 5), we can note that the presence of the shell does not imply a larger channel delay spread, as summarized in Table 2. It reports both the average value of the delay spread

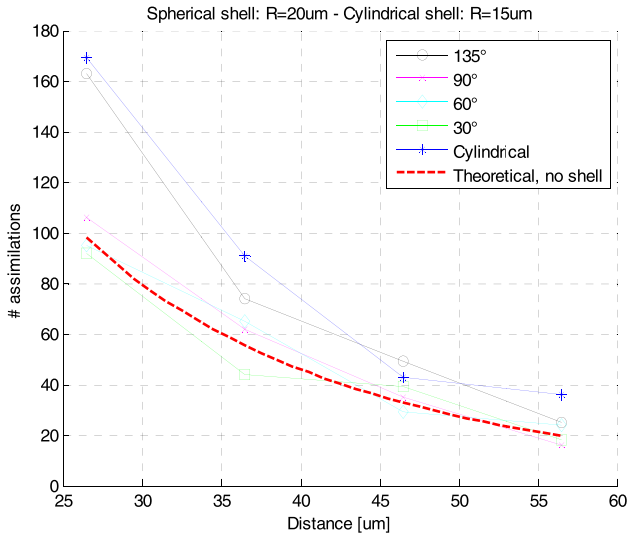

FIGURE 4. Average number of absorptions vs. d, for different configurations. The simulation time is equal to 10 s.

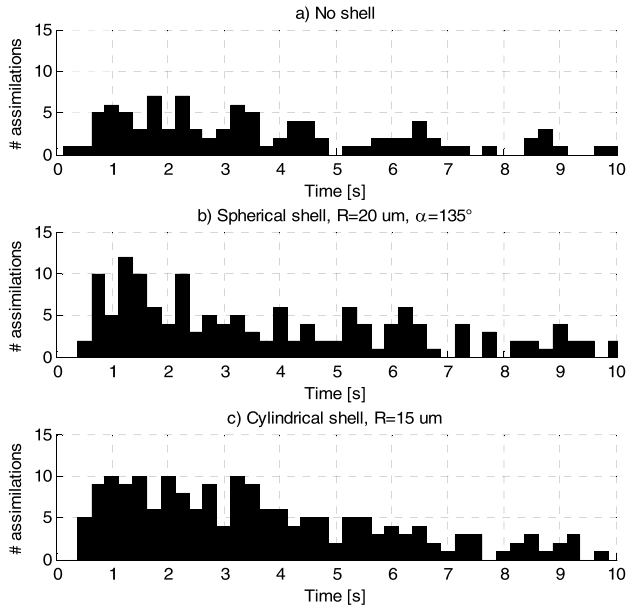

FIGURE 5. Absorption times for a) standard settings without shell, b) spherical cap shell with R = 20μm and $\alpha = 135°$, and c) cylindrical shell with R = 15μm and H = 30μm.

TABLE 2. Channel delay spread.

Configuration	Mean value	Standard deviation
No Shell	4.5375s	3.3278s
Spherical Shell	4.1975s	2.9331s
Cylindrical Shell	3.6584s	2.3736s

and its standard deviation. For both performance metrics, the presence of the shell provides significant benefits. In particular, it emerges that the more interesting configuration is, again, the cylindrical shell, which can ensure a decrease of the average delay spread equal to 20%, with also a decrease in the standard deviation of about 30%. Thus, not only the proposed technique is able to increase the receiver signal strength, but also it does not have any detrimental effect on the channel memory and thus on ISI. In any case, the contribution to the cannel memory can be controlled by means of ISI reduction techniques, such as the usage of enzymes [16].

B. SENSITIVITY TO MISALIGNMENT

Now, let us carry out an analysis on the effects that imperfect alignment, implemented by shell rotation, will produce on the carrier absorption, since it allows us investigating the directional properties of the proposed system. In this analysis, we have taken into account a few relevant rotation angles β for the cylindrical case only, since it outperforms the spherical cap one, as seen in previous performance figures.

In more detail, we have considered the case of misaligned cylinder with respect to the emission point, for both cylinder radius of $R = 5\mu$m and $R = 15\mu$m. The longitudinal axis of the cylinder is rotated by an angle β equal to 45°, 90°, and 180°, as depicted on Figure 6.b, Figure 6.c, and Figure 6.d, respectively.

The simulation results shown in Figure 7 indicate a significant decrease in the carrier assimilation profile as the rotation angle increases, making the cylindrical solution useless for rotation angles larger than 20°. In fact, for a misalignment smaller than 20°, the gain of the proposed solution is still significant with respect to the standard settings without any shell, with a gain roughly between 3dB ($\beta = 0$) and 1.5 dB ($\beta = 20°$). The worst case corresponds to a rotation angle $\beta = 180°$, where the receiver is able to absorb just 6 molecules with an emission burst of $Q = 2000$ nanoparticles.

Since this happens for both cylinder radii, this is a confirmation of the high directivity of the designed receiver system.

C. ASYMMETRIC CONFIGURATION

Finally, we have also relaxed the constraint of locating the center of the receiver node in the center of the cylinder. Thus, the cylinder is divided into two sections of different lengths, causing an asymmetrical positioning of the embedded receiver node. This means that, with respect to the receiver node, the whole cylinder length is split into two sections of different lengths, referred to as the front branch, of length L_F, and the bottom branch, of length L_B. The front branch is the part that has the basis open and exposed to the transmission point (see Figure 8).

Thus, depending on the considered configuration, the center of the receiver node can be shifted forward or backward along its longitudinal axis ($d_r \neq 0$ in Figure 8). Note that, for all configurations, in order to carry out a fair performance comparison, the communication distance does not change, so it is the cylinder that shifts on its axis with respect to the receiver node (i.e. d has the same value of the previous cases, see Figure 8). Also, in this new configuration, the receiver is always located on the cylinder axis, in order to guarantee

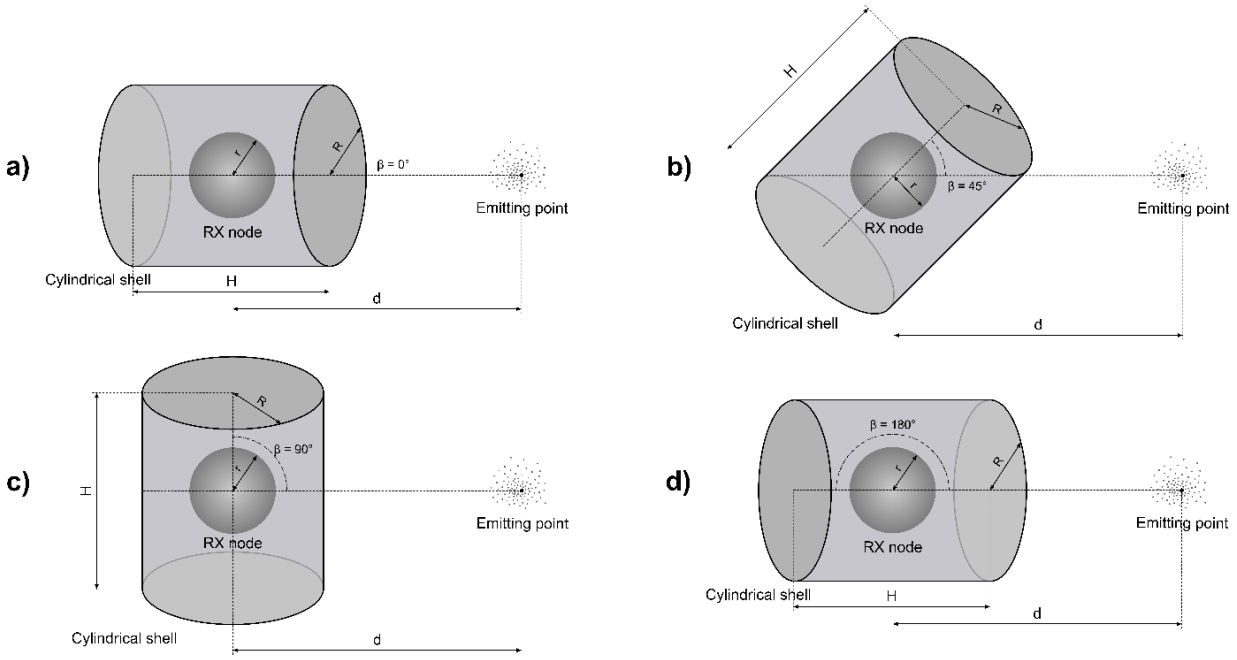

FIGURE 6. Different orientation for the cylindrical shell. a) cylinder aligned with the transmitter, b) cylinder rotated by $\beta = 45°$, c) cylinder rotated by $\beta = 90°$, and d) cylinder rotated by $\beta = 180°$, opposite to the transmitter.

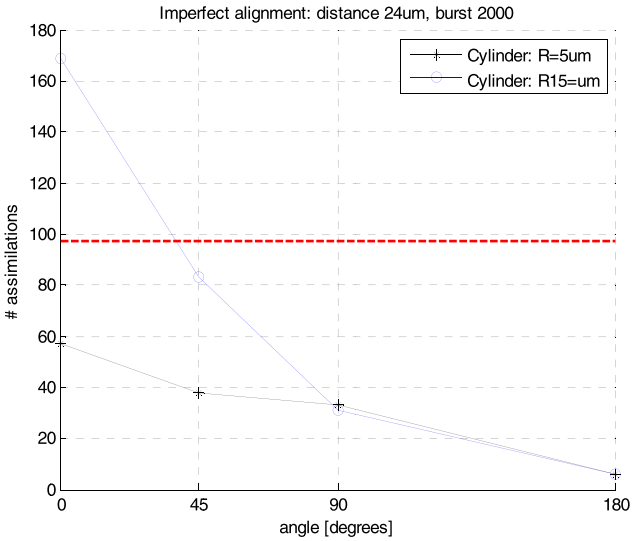

FIGURE 7. Average number of absorptions as a function of cylinder alignment, for two different aperture sizes. The red dashed line indicates the normal setting, without shells. The burst size is 2000 carriers. The simulation time is equal to 10.

equal opportunity to all the parts of the receiver to absorb carriers.

In what follows, we show the effects that a more general system configuration (i.e. the length of the front and back sections of the cylinder) may have on the assimilation profile at the receiver node. We have limited this analysis only to the configuration with $R = 15\mu$m, since it is the best performing one.

In addition to allow the center of the cylindrical shell and of the receiver to be shifted, we have also considered variations of the total length of the cylinder. In order to avoid any confusion, in this new set of experiments we have denoted the length of the cylinder, previously referred to as H, as L_{tot}. The resulting cylinder length L_{tot} is equal to

$$L_{tot} = L_F + L_{B+2r}, \tag{11}$$

as shown in Figure 8.

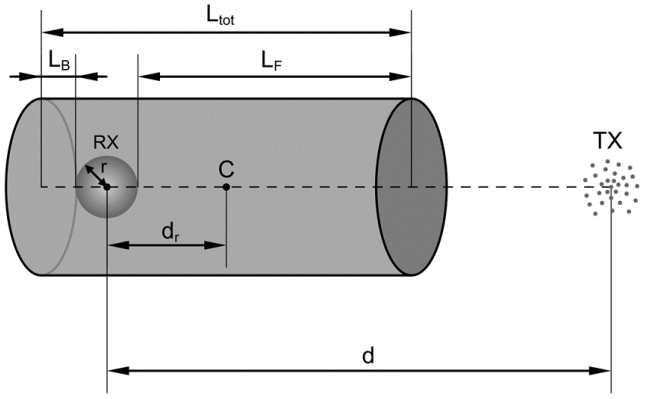

FIGURE 8. The center of the receiver node and the center of the cylindrical shell are shifted.

The selected values for both front and bottom branch lengths (L_F and L_B respectively) range from 0 to 22.5 μm.

This means that for the lowest value of L_B the cylinder basis is tangent to the receiver node surface.

The transmitter is located at a fixed distance d $= 26.5\mu$m from the receiver surface and releases a single burst $Q = 2000$ carriers, as in the previous experiments (see Table 1).

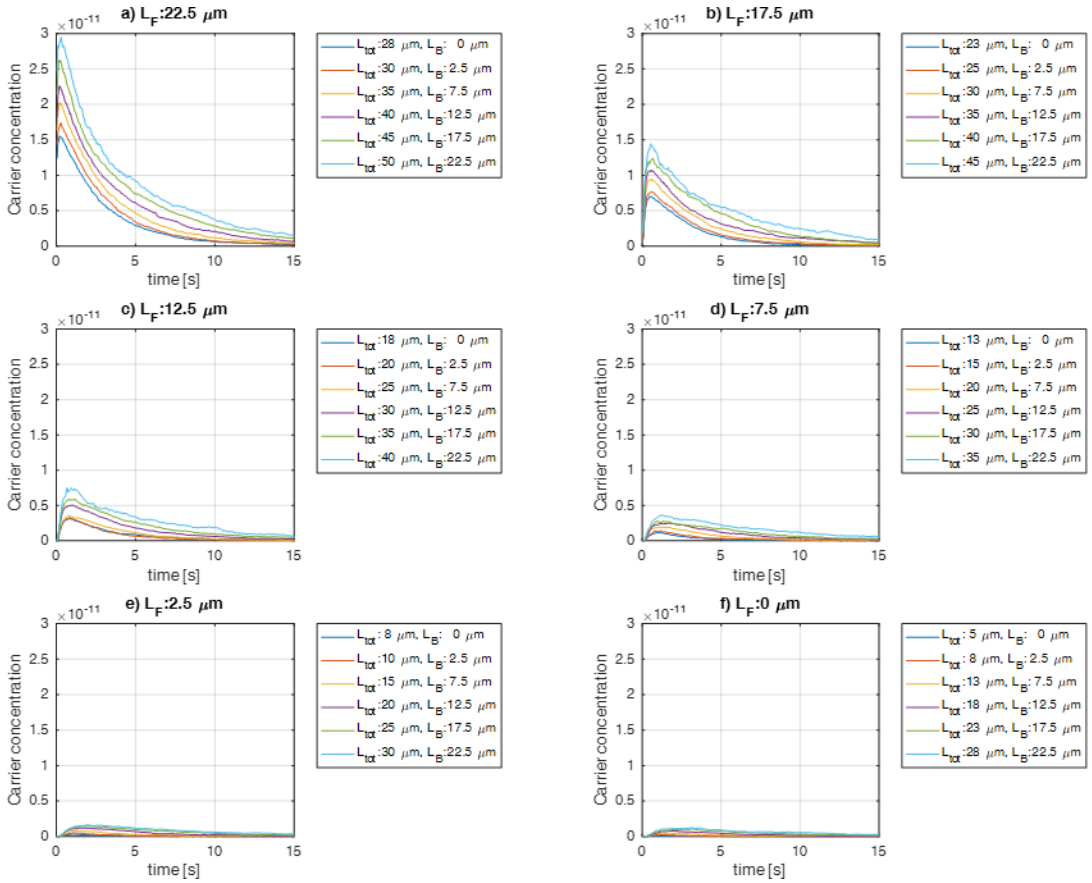

FIGURE 9. Carrier concentration for different configuration of L_F and L_B.

The results show that the concentration of carriers caught by the cylinder rises with the cylinder length, but the contribution given by the two lengths (L_F and L_B respectively) is not the same. In fact, the L_B term causes a slight curve shift on the carrier concentration profile and the L_F term always causes higher peak values, so the last contribution is more effective. This is evident in Figure 9, where we show the average carrier concentration inside the cylinder as a function of time.

This is an expected result, since high values of L_F imply that the front side of the cylinder is closer to the emission point, and, for this reason, it is able to collect and retain a larger number of carriers.

Having the same average carrier concentration does not necessarily imply comparable cylinder lengths. To clarify this point, let us consider the case shown in Figure 9.a, where the carrier concentration of 1.44×10^{-11} is reached at time $t = 0.55$ s by the configuration with $L_F = 22.5$ μm and $L_B = 0$ μm, and thus a total length $L_{tot} = 27.5$ μm. The same concentration is reached roughly at the same time instant for the configuration with $L_F = 17.5$ μm and $L_B = 22.5$ μm, resulting in a longer cylinder ($L_{tot} = 45$ μm), as shown in Figure 9.b. This means that in order to obtain a similar concentration value, in the second configuration mentioned above the bottom branch has to compensate the slightly shorter front branch (i.e. 17.5 μm) with the highest considered value (i.e. 22.5 μm), thus ensuring a consistent reservoir of carriers on the bottom section. As expected, a shorter front section corresponds also to a slight delay on the carrier harvesting, due to the time required by the carriers to propagate up to the front side of the cylinder before being conveyed by the cylinder itself to the receiver node.

The carrier concentration follows a predictable trend, as shown in Figure 9. However, the carrier assimilation on the receiver node does not follow the same trend, although an appreciable degree of correlation still exists with the number of carriers caught by the cylinder. In fact, the carrier assimilation depends also on the distance between the cylinder bottom surface L_B and the receiver node.

Figure 10 shows the assimilation profiles for different configurations of L_F and L_B compared with the theoretical curve (in red, no shell) over a simulation time of $t = 15$ s, as in Figure 9. Again, for reasonable times (i.e. lower than 15 s) the largest assimilation values are reached for $L_F = 22.5\mu$m and for small L_B values, that is for those ranging from 2.5 μm to 12.5 μm. However, looking at Figure 9.e and Figure 9.f, one can argue that, if the simulations lasted longer, it could turn out that high L_B values will yield even larger total assimilation values. Clearly, the very

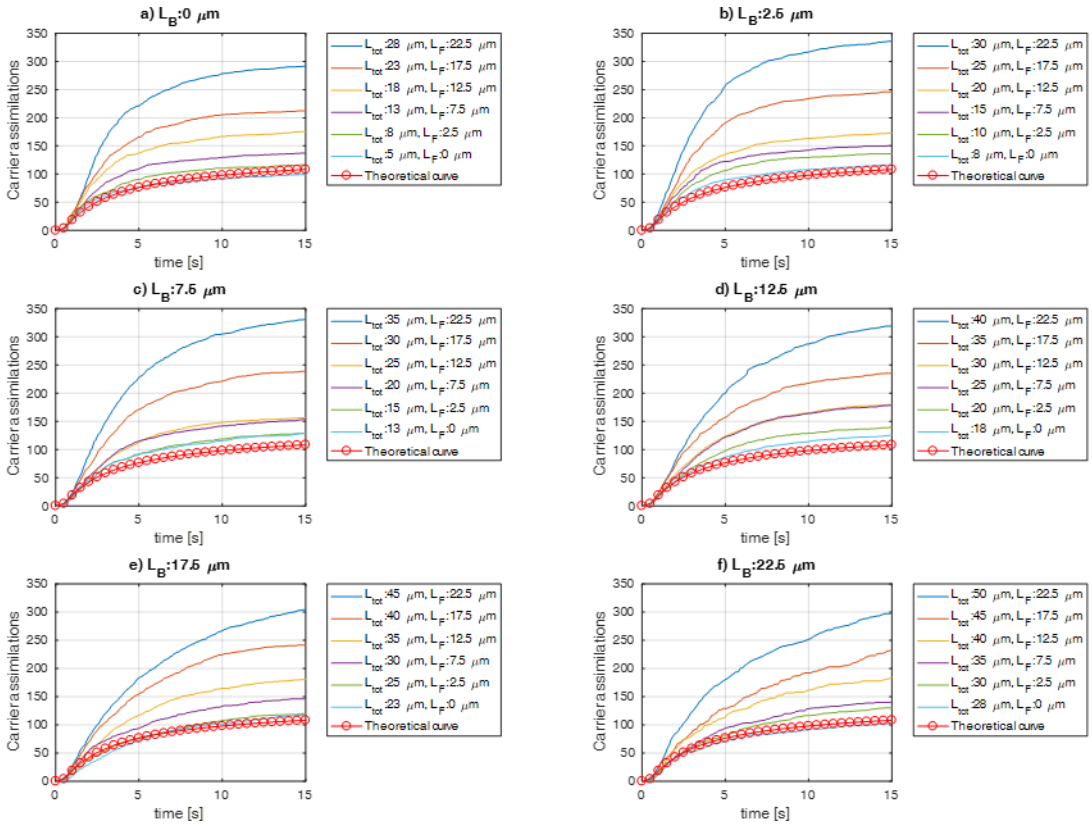

FIGURE 10. Carrier assimilations versus simulation time for different configurations of L_F and L_B.

long tail of their assimilation curve makes these configurations not appealing for setting up a reliable communication system, due to their exposure to ISI phenomenon, Thus, from now on we will focus mainly on low values of L_B.

Summing up, this means that the length of the bottom branch L_B affects the total number of assimilations and their assimilation profile over time, since the slope of the curve decreases as L_B increases. Moreover, for each configuration of L_F and L_B, the assimilation profiles are always higher than the theoretical case, that can only reach the same performance of the worst cases (i.e. $L_F = 0\mu$m for both $L_B = 0\mu$m and $L_B = 22.5\mu$m).

By itself, the metric measuring the total number of assimilations guarantees neither reliable communications, nor a significant advantage over a system without any shell. In order to obtain more insights, let us consider Figure 11, where we show the complementary assimilation fraction $f_A(t)$, defined as the complement of the ratio between the total assimilation $A(t)$ at current time t and its final value A_{tot}, estimated for t =15 s, whose value has been selected for the reasons explained above:

$$f_A(t) = 1 - A(t)/A_{tot}. \tag{12}$$

The results show the assimilation speed compared with the theoretical case (shown in red).

In these plots, the time required to absorb more than 90% the total assimilations is a function of the bottom length L_B. Again, limiting the observation time to 15 s, the best results are obtained for low L_B values ($L_B = [0; 2.5]\mu$m), as shown in Figure 11.a and Figure 11.b. This means that longer bottom branches will cause a spreading of the carriers along higher volumes and this will cause significant delays on the assimilation process. Thus, even if they, in principle, could guarantee the same or even higher values of total assimilations, they are not suitable for our goal.

This is an expected result, since the cloud of carriers has to propagate forward and then backward along the bottom branch of the cylinder. This means that, for higher assimilation values with respect to the theoretical case, the configurations with long bottom branches (e.g. Figure 10.e and Figure 10.f) necessarily require longer assimilation times, as shown on Figure 11.e and Figure 11.f. However, for short bottom branches, the time needed to reach 90% of assimilation is not only similar, but also lower than the configuration without shell, and this is an excellent result.

The time required to perform most of the overall assimilations is strictly related to the assimilation rates, as shown on Figure 12 for different configuration of L_F and L_B.

Again, the length of the front branch L_F still causes the higher assimilation peaks when L_F reaches the highest values. The simulation results show again that the length of the two branches affects the assimilation rate profile in two ways, changing the peak values and the slope of the curve.

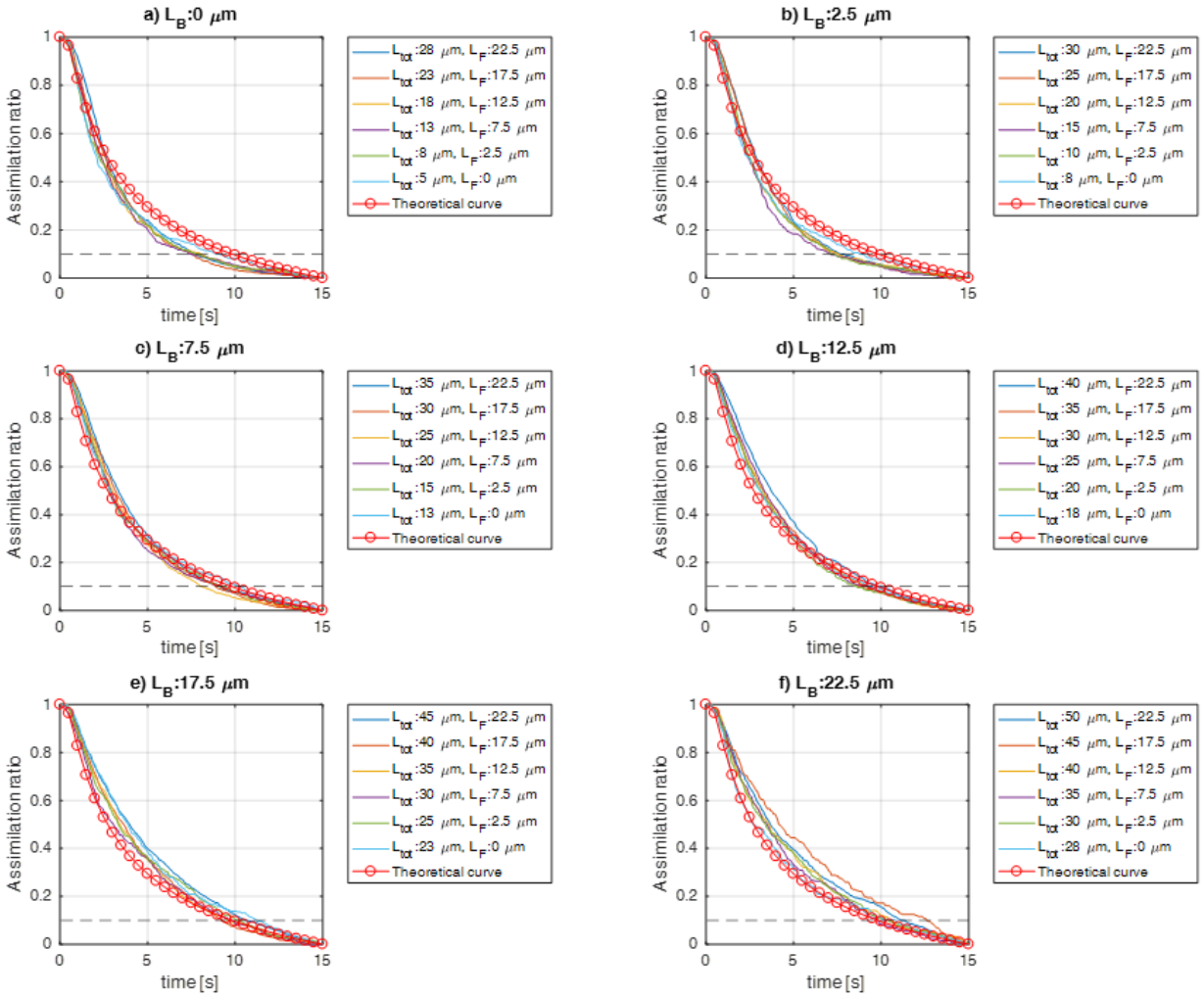

FIGURE 11. Assimilation ratio f_A versus simulation time; the crossing with the dashed black line (10% of residual carriers to assimilate within a time horizon of 15 s) provides an indication of the channel delay spread for the different configurations.

As a rule of thumb, we can conclude that L_F affects the peak values and L_B affects the slope of the curve, where higher values of L_B correspond to lower slopes, thus longer assimilation times.

This means that, for larger values of L_B, a consistent number of carriers is still trapped inside the bottom branch of the cylinder and a few sparse assimilations are still possible, causing assimilations for longer times.

Since these assimilation times are higher than the theoretical configuration (Figure 12.e and Figure 12.f), they cause the spreading of the shape of the received impulse, thus increasing the channel memory.

A further consideration related to the L_F values is that when the front side is close to the emission point, the cylinder can collect the carriers where their concentration is higher and, at the same time, it is able to forward them along its front branch in a sort of guided propagation, ensuring better performance compared with other configurations.

It is important to combine the assimilation rates (Figure 12) with the results shown in Figure 10, which depicts the absolute assimilation values for each cylinder configuration. In fact, in some cases (i.e. high values of L_B) the comparison provides additional insights: although assimilations occur slowly due to a long bottom branches, their actual final value could be higher than those obtained with other configurations, faster to reach the steady state of the assimilation profile.

Therefore, the profiles shown in Figure 11 provide information only about the speed to achieve their final assimilation values with respect to the case with no shell for a reasonable time interval. Combining these results with the assimilation rates of Figure 12, it is clear that over the tail (i.e. from $t = 10$ s to $t = 15$ s), there are still assimilations for each configuration of L_F and L_B, as well as for the configuration without the shell. The amount of these assimilations is more significant for higher values of L_B.

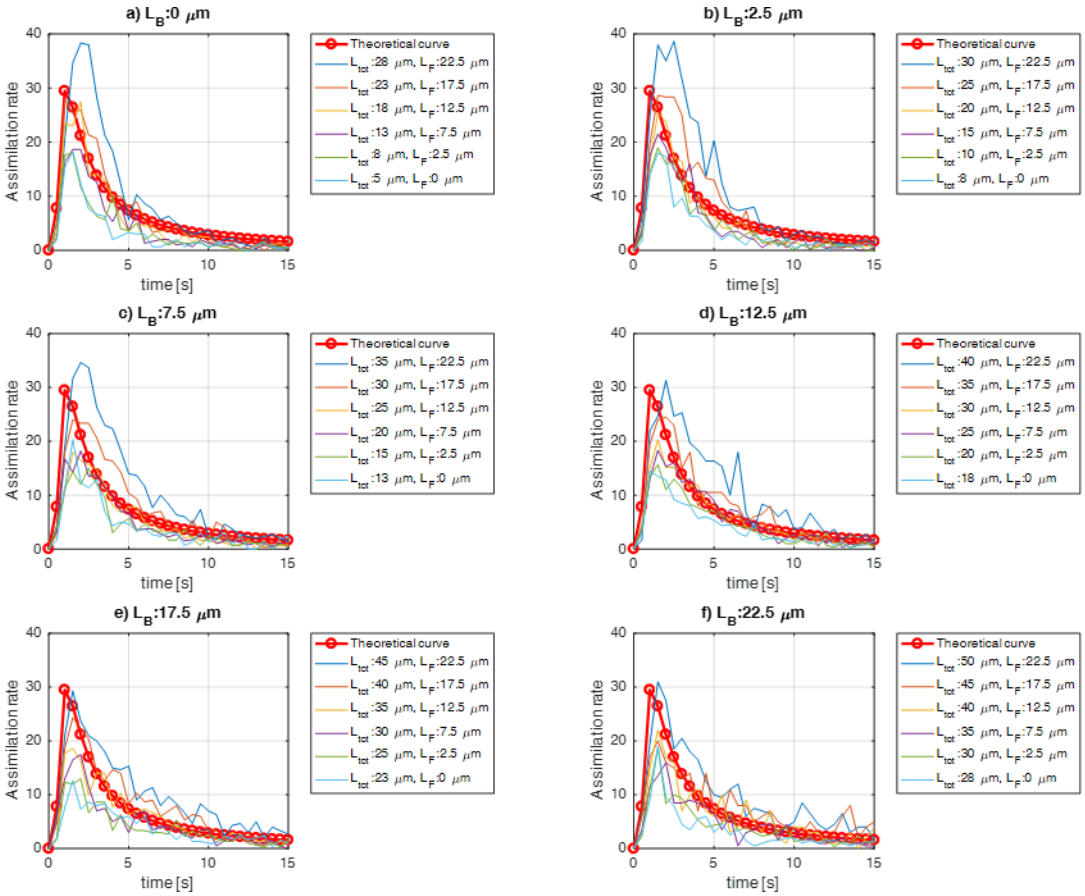

FIGURE 12. Carrier assimilation rate as a function of simulation time for different configurations of L_F and L_B.

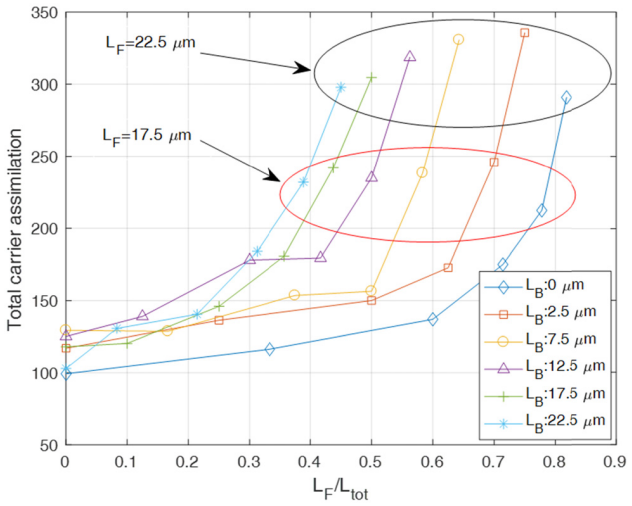

FIGURE 13. Carrier assimilation as a function of L_F/L_{tot}.

To conclude our analysis, Figure 13 highlights the importance of L_F over the cylinder length L_{tot}, showing that the best performance is obtained for larger values of L_F/L_{tot}, for any cylinder configuration.

Let us first consider the configuration for $L_F = 22.5\mu$m, highlighted by the top dashed ellipse. It results that the assimilation values rise from the lowest value (reached for $L_B = 0\mu$m) to the next value ($L_B = 2.5\mu$m) and then slightly decrease as L_B increases up to 22.5 μm.

To sum up, short bottom branches combined with long front branches should ensure ''high'' transmission rates on scenarios where the aim is the transmission of commands and information, whereas in those scenarios where the aim is the harvesting of carriers (i.e. molecules), longer bottom and front branches should ensure the highest number of absorptions.

The same profile is maintained by the value of $L_F = 17.5\mu$m (highlighted by the other dashed ellipse) even if the difference in the assimilation values are smaller. As L_F decreases, the assimilation curves are pushed down, thus reducing the relative differences. As mentioned above, under the same conditions, the highest assimilation values are reached for L_B that ranges from 2.5 μm to 7.5 μm.

The reason is that the bottom side of the cylinder is placed on a position that facilitates the bounce of the carriers back to the receiver node. This maintains a higher concentration of carriers close to the backside of the receiver node, and therefore it increases also the assimilations on that side, thus ensuring a fair occupation of the surface receptors. For the same reason, the lowest amount of assimilations corresponds

to $L_B = 0$. In fact, in this configuration the bottom side of the cylinder touches the receiver surface and this makes it difficult for the carriers to stay close to the receiving node and consequently to be absorbed.

A final remark on the results shown on Figures 9, 11 and 12 is that for the optimal configurations of L_B (i.e. from 2.5 μm up to 12.5 μm), the carrier concentration inside the cylinder tends to zero for longer simulation times (Figure 9). Moreover, also the assimilation rates in the tail are always lower than the theoretical case (no shell), showing that no significant assimilations should be expected for longer times (Figure 12). This proves also that these configurations require shorter assimilation times than the theoretical case for obtaining the same assimilations value normalized to their peak value (Figure 11), which, in turn, is definitely higher than the theoretical case.

This means that, for these cases, the channel memory is lower than in the theoretical case and for longer bottom branches, thus allowing the transmission of consecutive pulses with a limited impact on the ISI phenomena.

V. CONCLUSION

In this paper we have proposed a novel architecture for the receiving node of molecular communications in diffusive environments. It consists of equipping the receiving nanomachine with a reflector, able to trap the signal molecules for a while, giving them higher chances to be absorbed by the receiver positioned in a region surrounded by the reflecting shell.

We have used extensive simulation experiments to assess the effectiveness of the proposed solution. We have found that a significant gain of the received signal strength, in the order of 5.5 dB, can be achieved by using a cylindrical shell with unbalanced configuration (with $L_F \gg L_B$), with an aperture significantly larger than the receiver radius (the shell radius R is 6 times larger than receiver radius r). In addition, the gain achievable with the proposed receiver architecture is independent from the transmitter-receiver distance, which makes it appreciable.

The improvement is mainly due to both additional absorptions in the back surface of the receiver that, in a system without the shell, is the part with the lowest number of absorptions. The other significant contribution to assimilations is due to a front side aperture, which is located closer to the emission point, even if the distance between the receiver and the emission point is the same of the configuration without the reflecting shell. We have also evaluated the signal spread due to the trapping of molecules, and verified that the impact is not that negative, with an absorption profile comparable with that of the reference system, i.e. the receiver without any shell. In particular, the delay spread is slightly lower than it for the balanced cylinder case, and even lower for the unbalanced case with best performance, reporting at the same time higher transmission rates compared to the reference system. To sum up, our study on the accumulation of residual carriers inside the directional receiver system suggests a behavior not only similar but even better than that without any shell. In this regard, the usage of enzymes, able to remove the channel memory inside the receiving directional system, could minimize possible accumulations of residual carriers and thus further improve the system performance.

We stress that our results are slightly affected by the choice of limiting the observation time to 15 s, which seems to be a reasonable choice to estimate the tail of a symbol propagation in a molecular communication system. By this time interval, the tail of signal propagation in the unbalanced configuration with $L_F \gg L_B$ is practically exhausted, and the same holds for the configuration without shell. For other configurations this is not always true, thus we do not consider them suitable for a communication system.

Finally, we have verified that the overall system is not only able to increase the signal strength, but also highly directional. In fact, when the rotation of the shell aperture with respect to the perfect alignment with the emission point is larger than 20°, its effect becomes negligible with respect to the reference system. In addition, when the rotation is further increased to 90° and beyond, the number of absorbed nanoparticles tends to vanish, thus confirming the good directional properties of the receiving structure, which can allow implementing spatial division multiplexing in the molecular communication domain.

Some issues are still unexplored. In particular, technological alternatives to stick the receiver to the shell need to be explored, as well as mechanisms allowing the overall receiver plus shell structure to move in order to select the receiver orientation and thus obtain the desired performance.

REFERENCES

[1] J. Philibert, "One and a half century of diffusion: Fick, Einstein, before and beyond," *J. Basic Princ. Diffusion Theory, Exp. Appl.*, vol. 4, pp. 6.1–6.19, Sep. 2006.

[2] S. Kadloor, R. S. Adve, and A. W. Eckford, "Molecular communication using Brownian motion with drift," *IEEE Trans. Nanobiosci.*, vol. 11, no. 2, pp. 89–99, Jun. 2012.

[3] H. B. Yilmaz, A. C. Heren, T. Tugcu, and C.-B. Chae, "Three-dimensional channel characteristics for molecular communications with an absorbing receiver," *IEEE Commun. Lett.*, vol. 18, no. 6, pp. 929–932, Jun. 2014.

[4] A. Akkaya, H. B. Yilmaz, C. Chae, and T. Tugcu, "Effect of receptor density and size on signal reception in molecular communication via diffusion with an absorbing receiver," *IEEE Commun. Lett.*, vol. 19, no. 2, pp. 155–158, Feb. 2015.

[5] L. Felicetti, M. Femminella, and G. Reali, "A simulation tool for nanoscale biological networks," *Nano Commun. Netw.*, vol. 3, no. 1, pp. 2–18, 2012.

[6] L. Felicetti, M. Femminella, and G. Reali, "Simulation of molecular signaling in blood vessels: Software design and application to atherogenesis," *Nano Commun. Netw.*, vol. 4, no. 3, pp. 98–119, 2013.

[7] L. Felicetti, M. Femminella, G. Reali, P. Gresele, and M. Malvestiti, "Simulating an *in vitro* experiment on nanoscale communications by using $BiNS_2$," *Nano Commun. Netw.*, vol. 4, no. 4, pp. 172–180, 2013.

[8] L. Felicetti, M. Femminella, G. Reali, J. N. Daigle, M. Malvestiti, and P. Gresele, "Modeling CD40-based molecular communications in blood vessels," *IEEE Trans. Nanobiosci.*, vol. 13, no. 3, pp. 230–243, Sep. 2014.

[9] D. Gidaspow and J. Huang, "Kinetic theory based model for blood flow and its viscosity," *Ann. Biomed. Eng.*, vol. 37, no. 8, pp. 1534–1545, Aug. 2009.

[10] W. Guo, S. Wang, A. Eckford, and J. Wu, "Reliable communication envelopes of molecular diffusion channels," *Electron. Lett.*, vol. 49, no. 19, pp. 1248–1249, Sep. 2013.

[11] D. Kilinc and O. B. Akan, "Receiver design for molecular communication," *IEEE J. Sel. Areas Commun.*, vol. 31, no. 12, pp. 705–714, Dec. 2013.
[12] M. Ş. Kuran, H. B. Yilmaz, T. Tugcu, and B. Özerman, "Energy model for communication via diffusion in nanonetworks," *Nano Commun. Netw.*, vol. 1, no. 2, pp. 86–95, 2010.
[13] M. U. Mahfuz, D. Makrakis, and H. T. Mouftah, "A comprehensive study of sampling-based optimum signal detection in concentration-encoded molecular communication," *IEEE Trans. NanoBiosci*, vol. 13, no. 3, pp. 208–222, Sep. 2014.
[14] M. U. Mahfuz, D. Makrakis, and H. T. Mouftah, "On the characterization of binary concentration-encoded molecular communication in nanonetworks," *Nano Commun. Netw.*, vol. 1, no. 4, pp. 289–300, 2010.
[15] L. S. Meng, P. C. Yeh, K. C. Chen, and I. F. Akyildiz, "On receiver design for diffusion-based molecular communication," *IEEE Trans. Signal Process.*, vol. 62, no. 22, pp. 6032–6044, Nov. 2014.
[16] A. Noel, K. C. Cheung, and R. Schober, "Improving receiver performance of diffusive molecular communication with enzymes," *IEEE Trans. NanoBiosci.*, vol. 13, no. 1, pp. 31–43, Mar. 2014.
[17] M. Pierobon and I. F. Akyildiz, "A statistical–physical model of interference in diffusion-based molecular nanonetworks," *IEEE Trans. Commun.*, vol. 62, no. 6, pp. 2085–2095, Jun. 2014.
[18] H. ShahMohammadian, G. G. Messier, and S. Magierowski, "Optimum receiver for molecule shift keying modulation in diffusion-based molecular communication channels," *Nano Commun. Netw.*, vol. 3, pp. 183–195, Sep. 2012.
[19] H. B. Yilmaz and C. B. Chae, "Simulation study of molecular communication systems with an absorbing receiver: Modulation and ISI mitigation techniques," *Simul. Model. Pract. Theory*, vol. 49, no. 15, pp. 136–150, 2014.
[20] G. Wei and R. Marculescu, "Miniature devices in the wild: Modeling molecular communication in complex extracellular spaces," *IEEE J. Sel. Areas Commun.*, vol. 32, no. 12, pp. 2344–2353, Dec. 2014.
[21] Z. Bao *et al.*, "Chemical reduction of three-dimensional silica microassemblies into microporous silicon replicas," *Nature*, vol. 446, pp. 172–175, Mar. 2007.
[22] L. Felicetti, M. Femminella, and G. Reali, "Smart antennas for diffusion-based molecular communications," in *Proc. ACM NANOCOM*, Boston, MA, USA, 2015, Art. no. 27.
[23] W. Guo *et al.*, "SMIET: Simultaneous molecular information and energy transfer," *IEEE Wireless Commun.*, vol. 25, no. 1, pp. 106–113, Feb. 2018.
[24] W. Guo, C. Mias, N. Farsad, and J.-L. Wu, "Molecular versus electromagnetic wave propagation loss in macro-scale environments," *IEEE Trans. Mol. Biol. Multi-Scale Commun.*, vol. 1, no. 1, pp. 18–25, Mar. 2015.
[25] Y. J. Cho, H. B. Yilmaz, W. Guo, and C.-B. Chae, "Effective enzyme deployment for degradation of interference molecules in molecular communication," in *Proc. IEEE Wireless Commun. Netw. Conf. (WCNC)*, San Francisco, CA, USA, Mar. 2017, pp. 1–6.
[26] H. B. Yilmaz, G.-Y. Suk, and C.-B. Chae, "Chemical propagation pattern for molecular communications," *IEEE Wireless Commun. Lett.*, vol. 6, no. 2, pp. 226–229, Apr. 2017.
[27] N. Farsad, H. B. Yilmaz, A. Eckford, C.-B. Chae, and W. Guo, "A comprehensive survey of recent advancements in molecular communication," *IEEE Commun. Surveys Tuts.*, vol. 18, no. 3, pp. 1887–1919, 3rd Quart., 2016.
[28] L. Felicetti, M. Femminella, G. Reali, and P. Liò, "Applications of molecular communications to medicine: A survey," *Nano Commun. Netw.*, vol. 7, pp. 27–45, Mar. 2016.
[29] A. Ahmadzadeh, H. Arjmandi, A. Burkovski, and R. Schober, "Comprehensive reactive receiver modeling for diffusive molecular communication systems: Reversible binding, molecule degradation, and finite number of receptors," *IEEE Trans. Nanobiosci.*, vol. 15, no. 7, pp. 713–727, Oct. 2016.

L. FELICETTI received the master's degree in information and communication engineering from the University of Perugia, in 2011, and the Ph.D. degree in information engineering, in 2015. He is currently a Postdoctoral Researcher with the Department of Engineering, University of Perugia. His current research interests focus on nanoscale networking and communications.

M. FEMMINELLA (M'01) received the master's and Ph.D. degrees in electronic engineering from the University of Perugia, in 1999 and 2003, respectively. Since 2006, he has been an Assistant Professor with the Department of Engineering, University of Perugia. He has co-authored about 100 papers in international journals and refereed international conferences. His current research interests focus on nanoscale networking and communications, big data systems, and network and service management architectures and protocols for 5G networks.

G. REALI received the Ph.D. degree in telecommunications from the University of Perugia, in 1997. From 1997 to 2004, he was a Researcher with the Department of Electronic and Information Engineering, University of Perugia. In 1999, he visited the Computer Science Department, UCLA. He has been an Associate Professor with the Department of Engineering, University of Perugia, Italy, since 2005. His research activities include resource allocation over packet networks, wireless networking, network management, multimedia services, big data management, and nanoscale communications.